

POWER GENERATION FROM COMBUSTED “SYNGAS” USING HYBRID THERMOELECTRIC GENERATOR AND FORECASTING THE PERFORMANCE WITH ANN TECHNIQUE

Appadurai Anitha Angeline^{1,*}, Jayaraj Jayakumar¹, Lazarus Godson Asirvatham²,
Somchai Wongwises^{3,4}

ABSTRACT

Gasification and combustion of de-oiled Pongamia Pinnata seed cake is done to produce higher energy biomass waste heat “syngas” for generating power using hybrid thermoelectric generator (TEG). A test rig is fabricated and experiments conducted with synthetic oil (*Therminol-55*) as the heating fluid under water and air-cooled methods. The hot side temperature is varied from 200 - 250°C while the coolant temperature is maintained at 30 °C for both water and air respectively. Experimental results showed 22.27% enhancement in electric power at a constant hot side temperature of 250 °C under water cooled method. In addition, simulation results for the above mentioned conditions using artificial neural networks (ANN) tool in *MATLAB* also agreed well with the sample experimental results. The performance parameters such as open circuit voltage, maximum output power and matched load resistance are forecasted using ANN upto maximum possible hot side temperature of 350°C. Further, the financial evaluation of Biomass gasified-thermoelectric system (\$0.0018/kWh and in terms of Indian currency is Rs 0.0676/kWh) is found to be almost negligible on comparison with other available renewable energy technologies.

Keywords: *Pongamia, ANN, Hybrid, Performance Parameters, Synthetic Oil, Thermoelectric Generator, Cost Analysis*

INTRODUCTION

Despite cyclic changes in climate, generating stations such as thermal, nuclear and geothermal power plants and large scale industries such as automobile, glass and aluminum factories, waste incinerators operate incessantly every day, all through the year. These systems give out very high temperature heat as losses to the atmosphere. In reality, this high temperature waste heat (about 450 – 650°C) is absorbed using cold water and sent out to the surroundings as medium temperature waste heat (about 250 – 350°C) which can be used for directly converting heat to electricity using the thermoelectric generator. Employing synthetic oil as heating fluid rather than using ordinary water, results in increased heat transfer rate and is suitable for temperatures upto 350°C at atmospheric pressure conditions. This recovered energy can either be harvested or stored in batteries to power small equipments or used for lighting purposes.

Several researchers have analytically and experimentally studied the performance of different commercially available thermoelectric generators using waste heat from automobiles, biomass cook stoves, heat lost from solar panels and so on. Some of their findings are briefly discussed:

Prakash et al [1] recovered the surface waste heat of an IC engine using thermoelectric generators and observed that about 4 to 9W of power is obtained from a 4×4 cm² surface area of silencer. Su et al [2] developed a prototype “Warrior” for harvesting waste energy from automobiles. The performance parameters at 312°C hot side temperature and 69°C cold side temperature were analyzed using the revolving drum test. Chandy et al [3] developed an Automobile Exhaust Thermoelectric heat exchanger system using ANSYS and analyzed its performance at 269K cold side temperature and 600 - 1200K hot side temperatures. Results showed that the overall performance of the system increased with increase in engine speed and a 64.6% enhancement in voltage was observed when the hot side temperature varied from 600 – 1200K.

This paper was recommended for publication in revised form by Regional Editor Balaram Kundu

¹Department of Electrical and Electronics Engineering, Karunya University, Coimbatore, Tamil Nadu, India;

²Department of Mechanical Engineering, Karunya University, Coimbatore, Tamil Nadu, India

³Fluid Mechanics, Thermal Engineering and Multiphase Flow Research Lab. (FUTURE), Department of Mechanical Engineering, Faculty of Engineering, King Mongkut's University of Technology Thonburi, Bangmod, Bangkok 10140, Thailand.

⁴The Academy of Science, The Royal Institute of Thailand, Sanam Suea Pa, Dusit, Bangkok 10300, Thailand

*E-mail address: anitha_angeline@karunya.edu.in;

Manuscript Received 8 August 2017, Accepted 18 October 2017

Deok et al [4] connected two types of thermoelectric modules to the exhaust port of the diesel engine and studied the various performance characteristics using different shapes of heat sinks at different thermal conditions. It was observed that the rectangular heat sink produced maximum power output with 11.29% increase in power when compared with that of forward and reverse –facing triangular prism heat sinks at 80°C cold side temperature. Liu et al [5] proposed a two-stage thermoelectric generator connected to the vehicle exhaust pipe using a heat pipe and found that a maximum power of 250W and an enhanced thermal efficiency of 5.37% were obtained at the hot side temperature of 473K. Liu et al [6] conducted experiments on a novel prototype active solar thermoelectric radiant wall (*ASTRW*) system for winter operation modes. Results showed that the *ASTRW* system not only eliminates conventional building thermal losses but also provide a heating capacity for space heating. As the solar irradiation intensity increases, the interior surface temperature of the *ASTRW* system also increased

Alomair et al [7] developed a solar –thermoelectric liquid chiller (*STLC*) system and analyzed the performance analytically and experimentally at different temperature conditions. It was observed that the heat removal rate of the *STLC* system increases with increasing bulk temperature of the chiller unit. Liu et al [8] proposed a new active solar thermoelectric radiant wall (*ASTRW*) system that reduces general requirements of the air conditioning system in which the mean inner surface temperature of the system was found to be lower than that of the room temperature. Özdemir et al [9] modeled a solar heating thermoelectric generator employing a cooling wind chimney for effective electrical power generation. The generated power output depends upon the temperature differences available across the modules. Liu et al [10] conducted experiments on a prototype solar-thermoelectric cooled ceiling along with displacement ventilation (*STCC-DV*) system under heating and cooling modes. Results showed that any decrease in the temperature difference between ambient and indoor temperature, leads to a significant increase in the total heat flux and a co-efficient of performance in both the heating and cooling modes.

Killander and Bass [11] integrated two thermoelectric generators placed on an aluminum plate, on the outer walls of a wood-fed stove in Northern Sweden. During the early hours, the thermoelectric generator output was about 10W as the ambient temperature was less and the wooden stove was being kindled regularly. When the temperature became steady during the day, the generator output varied between 4-7W. Shaughnessy et al [12] integrated a thermoelectric generator to a portable cooking stove. For testing purpose, original heat source was replaced by cartridge heaters with variable power supply and the cold side temperature was maintained constant using a water flow loop. An output of 3.9W was obtained at a temperature difference of 230°C. Champier et al [13] connected four peltier modules in series and placed it on top of an aluminum block supplied by a 2.2kW gas heater. The individual performance of each module was verified and the maximum power output of each module was found to vary between 1.7 - 2.3W. The net series power output of the four modules was about 7W. Rida et al [14] integrated a thermoelectric generator to the side walls of a wooden stove and obtained an output power of 4.2W at a temperature gradient of about 152°C. Lertsatithanakorn [15] studied the performance of a thermoelectric generator integrated to a biomass cook stove (*BITE*) that produced about 2.4W at 150°C temperature difference which was adequate to run a small radio or light an incandescent light bulb.

Moreover, a theoretical study has been carried out by the present authors using the hybrid *TEG*. The hot side temperature is varied upto 350°C and a maximum power output of 21.7W was attained at maximum allowable hot side temperature (350°C) and minimum allowable cold side temperature (30°C) at a matched load resistance of 0.97Ω [16,31]. Similar studies have also been carried out by different authors [17-30,43].

Based on the above mentioned literature, it is pragmatic that the researchers have performed experimental investigations on recovered waste heat from biomass cookstoves, automobile exhaust, heat lost from solar panels for power generation using Bismuth Telluride thermoelectric generators. It is reported that the thermoelectric power generated varied from 0.5W to 5.3W for an average temperature difference of 80 – 200°C. Furthermore, very few work has been reported till date in open literature based on power generation using a hybrid thermoelectric generator and synthetic oil as heat transfer liquid. Besides, the obtained experimental results clearly indicate that the power generation rate increases with increase in thermoelectric generator hot side temperature for a fixed cold side temperature. But there are certain problems faced by the researchers while performing experiments : huge system losses due to energy imbalance, heat lost to the surroundings due to improper insulation, increase in thermal contact resistances owing to less clamping force, inaccurate measurement of hot and cold side temperatures using thermocouples that are inserted into heating blocks leading to non-uniform surface temperature distribution, non-uniform material properties due to uncertainties in the manufacturing process. These shortcomings lead to reduced performance of the thermoelectric generators. To overcome these drawbacks, Artificial Neural Networks (*ANN*) is

one of the most effective and efficient ways of predicting the performance of thermoelectric generators with high prediction accuracy.

In the present work, an experimental test facility is fabricated. It is suggested that gasified Pongamia de-oiled seed cake, on combustion produces higher energy biomass waste heat (250 – 350°C) which can be used for power generation using the thermoelectric system. Based on the obtained temperature range, laboratory based experiments are carried out at the hot side temperature ranging from 200 – 250°C and the coolant temperature maintained at ambient conditions (about 30°C). *Therminol-55* is used as the heat transfer fluid over the hot side with water and air cooled techniques employed over the cold side. Using the sample experimental values, the artificial neural networks tool in *MATLAB* is utilized and the performance of the hybrid thermoelectric generator (*TEG1-PB-12611-6.0*) at the hot side temperatures ranging from 200 – 250°C and at ambient cold side conditions (about 30°C) is analyzed. The simulated ANN parameters are compared with sample experimental results and based on the closeness between both the methodologies; the performance of thermoelectric system employing synthetic oil as heat transfer fluid (upto a maximum temperature gradient of 320°C) is estimated even without actually performing the experiments.

BIOMASS WASTE MANAGEMENT

Non-edible oil from *Jatropha (Jatropha curcas)* and *Karanja (Pongamia pinnata)* plants are recognized as India's main source of biodiesel production (Planning Commission, Government of India, 2003). One hectare of cultivated Pongamia Pinnata trees supply about 7.7 tons of Pongamia seeds that can yield 1.8095 tons of Pongamia oil and 5.8905 tons of de-oiled seed cake [32]. The de-oiled seed cakes can neither be used as animal feed or fertilizer due to its bitterness and toxicity. Hence, disposal of these de-oiled cakes is of huge concern. It is, therefore, recommended to use this de-oiled seed cake for syngas generation. Gasification of the de-oiled Pongamia seed cake results in production of "syngas". The generated synthesis gas can be directly used for operating engines, heating, lighting and cooking purposes. Heat energy produced on combustion of generated "syngas" can be used for direct conversion of heat into electricity using a thermoelectric generator. The slag left behind gasification process, when mixed with cow-dung can be used as an organic fertilizer. Figure 1 gives the details on how the de-oiled cakes can be utilized.

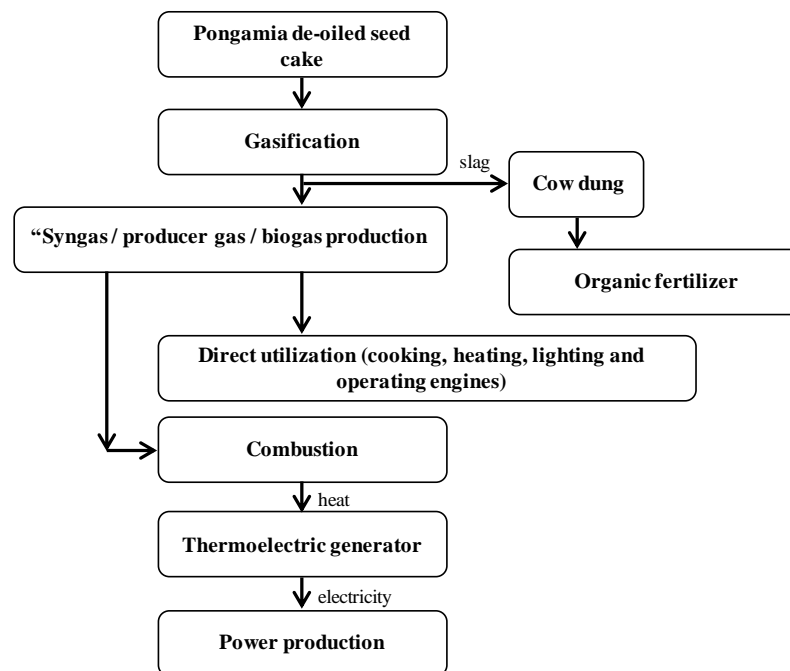


Figure 1. Utilization of Pongamia de-oiled seed cake

The future scenario of the production and utilization of non-edible seeds for biodiesel production in India is going to grow tremendously with time [33]. It is projected that 145 kilometric tons of Pongamia seed is produced every year in India [34]. Hence, waste management plays an important role in managing waste from the inception to its final disposal.

GASIFICATION PROCESS

Pongamia de-oiled seed cake is gasified at 700°C using a fluidized bed reactor in which the biomass based carbon-rich material is converted into a resultant gas mix “syngas”, a combination of carbon monoxide and hydrogen. Combustion of the resultant gas mix “syngas” resulted in pollution free, low-cost heat energy (renewable) as the gasified compounds are obtained from organic biomass [35]. Proximate and Ultimate Analysis of Pongamia de-oiled seed cake is done and the results obtained are given in Table 1. On combustion of the collected “syngas”, a temperature of about 250 - 350°C is achieved. This heat energy can be given as an input to the hot side of the hybrid TEG unit. For experimentation purpose, the heat energy generated by combustion of gasified Pongamia de-oiled seed cake is mimicked by an electrical heater.

Table 1. Proximate and Ultimate Analysis of Pongamia de-oiled seed cake

Proximate Analysis	(wt%)	Ultimate Analysis	(wt%)
Moisture	7.09	Moisture	7.09
Ash	3.53	Mineral matter	7.80
Volatile Matter	78.03	C	65.84
Fixed Carbon	11.35	H	6.5
		N	4.5
		S	1.37
		O	6.0
		GCV (Kcal/kg)	4622

GAS CHROMATOGRAPHY

Gas chromatography is usually done to separate and analyze the different compounds that can be vaporized without any decomposition at higher temperatures. When the gas mixture is separated into individual components, it is easy to qualitate and quantitate the amount of the individual samples present in the mixture. Initially, the biomass waste is burnt in a reactor which is powered by a dimmerstat. The gases obtained are collected in a bladder through a gas tube. The obtained gas mixture is connected to the gas chromatograph for separation and further analysis. Figure 2 shows the main structure of a basic gas chromatograph.

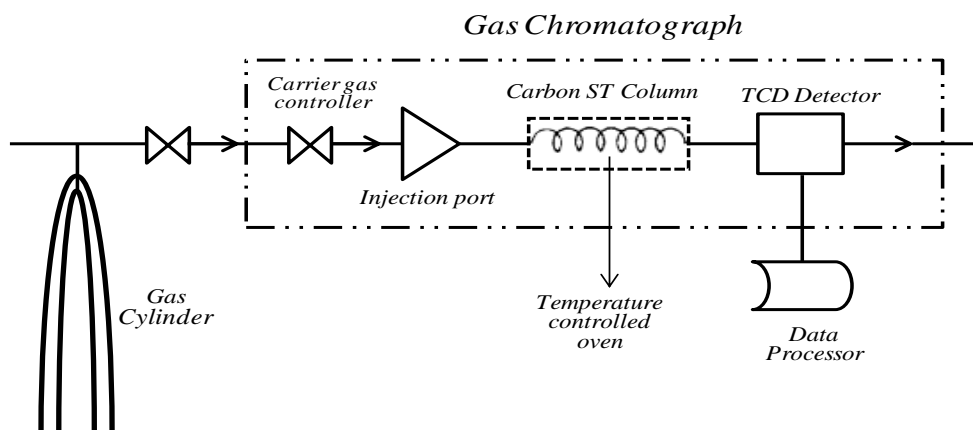


Figure 2. Process structure of a basic gas chromatograph.

The gas samples were analyzed using SHIMADZU GC-2014 equipped with TCD detector and shin carbon ST column (100/120 mesh, 2 m and 1 mm I.D). Nitrogen is used as the carrier gas and the flow rate is maintained at 10 ml min⁻¹. The nitrogen gas is passed through the purifier before entering in GC and gas sample (about 0.5 ml) is injected into the injection port using a gas sampler. The gas samples are vaporized in the injection port. The vaporized gases (solutes) are transferred to the column using the carrier gas. The column is usually placed in a temperature controlled oven and the oven temperature is kept at 40°C for 3 minutes and then raised to 250°C at a rate of 8°C min⁻¹ and then the same temperature is maintained for about 10 minutes. Now, the solutes move through the column at different rates. The fastest moving solute leaves the column first pursued by the other solutes in the consequent order. The standard gas with known composition is used for calibration prior to the analysis of gas samples. The eluted solutes enter the heated detector. When a solute hits the detector, a signal is being generated. The size of the generated electronic signal is recorded using a data processor and a graph is plotted against the

elapsed time to create a chromatogram. The chromatogram of syngas obtained by gasification of Pongamia de-oiled seed cake is shown in Figure 3. The details of the concentration and peak retention time of the various gas components are given in Table 2. The various syngas compositions generated at 700°C and ER 0.19 is tabulated in Table 3.

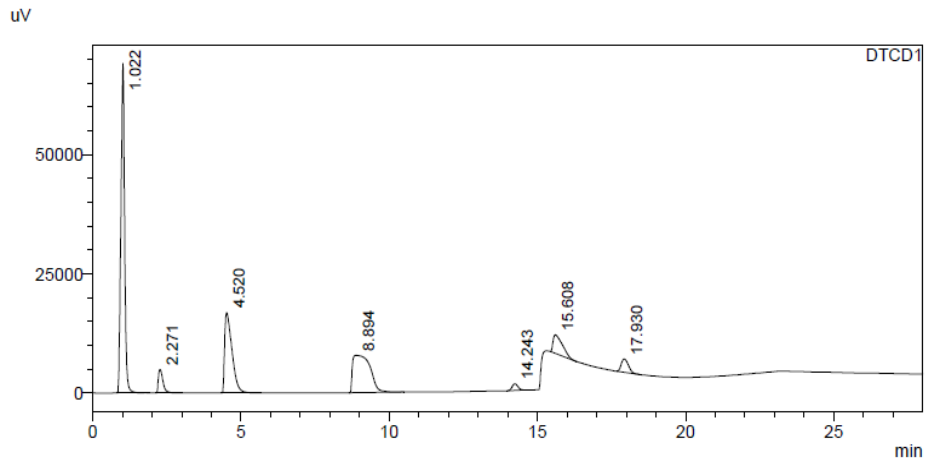


Figure 3. Chromatogram of “syngas” by gasification of Pongamia de-oiled seed cake

Table 2. Peak Values of “syngas” components

Peak No	Name	Retention Time	Concentration	Unit	Area (mm ²)	Height (mm)
1	H ₂	1.022	8.744	%	594441	69002
2	CO	2.271	9.656	%	53407	4914
3	CH ₄	4.520	7.118	%	291268	16825
4	CO ₂	8.894	8.603	%	323265	7083
5	C ₂ H ₂	14.243	0.428	%	18934	1395
6	C ₂ H ₄	15.608	6.510	%	86729	3874
7	C ₂ H ₆	17.930	1.541	%	46764	2787
Total					1414809	106600

Table 3. “Syngas” compositions generated at 700°C, ER 0.19

Gas Composition (mole %) and Lower heating value (LHV)							
H ₂	CO	CO ₂	CH ₄	C ₂ H ₂	C ₂ H ₄	C ₂ H ₆	LHV (MJ/Nm ³)
8.744	9.656	8.603	7.118	0.428	6.51	1.541	5.22

EXPERIMENTAL INVESTIGATION

In order to study the performance of the hybrid thermoelectric generator at different temperatures, an experimental test facility is fabricated. The schematic of the experimental test facility is given in Figure 4. The details of fabrication of test facility are published elsewhere [36]. The solid copper block is replaced by an equivalent hollow copper block filled with synthetic oil (*Therminol-55*). It consists of a hollow copper block, hybrid *TEG*, heat exchanger, external load resistance and a data acquisition unit. The hybrid *TEG* is placed between the hollow copper block over the hot side and a heat exchanger on the cold side. Two Cartridge heaters with variable power supply are placed inside the hollow copper block filled with heating fluid to maintain a temperature gradient across the hybrid *TEG*. The whole *TEG* unit is insulated using ceramic wool to avoid the heat loss into the atmosphere. The hybrid *TEG* module is held tightly between the copper block on the hot side and a heat exchanger unit on the cold side of the hybrid *TEG* module by compression method. Clamping is done using two stainless steel screws of 5mm diameter on either side of the hybrid *TEG* at a distance of 0.5inches from the sides of the *TEG* with 0.3kgm torque per screw. A clamping force of 5kgs is applied to hold tightly the hybrid *TEG* module in order to reduce the thermal contact effect. The pressure load is calculated to be 0.176kgcm⁻² based on the applied 5kg weight. The screws were tightened evenly in small increments. The design, screw diameter, number of screws and the torque per screw are chosen based on the power module installation notes supplied by Thermal Electronics Corporation, Canada.

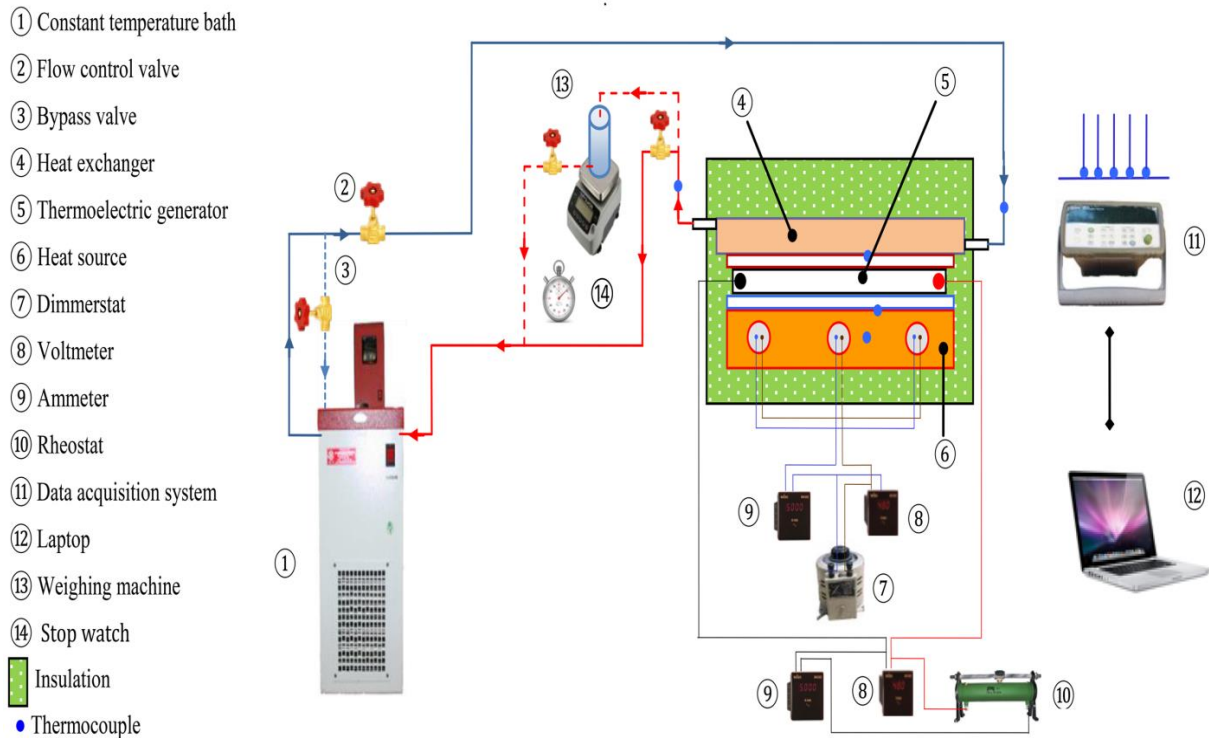


Figure 4. Schematic of the experimental test-rig

The hybrid thermoelectric generator comprises of p-type lead telluride and n-type Bi_2Te_3 semiconductor material and offers superior performance over 260°C hot side temperature. The hybrid thermoelectric generator *TEG1-PB-12611-6.0* supplier specifications are given in Table 4. Heat is supplied to the hot side of the hybrid TEG using cartridge heaters placed inside the synthetic oil filled hollow copper block and powered by a variable power source. By adjusting the power input to the cartridge heaters, different temperature gradients across the hybrid TEG module is obtained. Both water and air cooling methods are employed over the cold side. The hot and cold side temperatures are observed using micro T-type thermocouples.

Table 4. Supplier Specifications - *TEG1-PB-12611-6.0*

Parameters	Hybrid TEG
Model Number	TEG1-PB-12611-6.0
Composition	Bi_2Te_3 - PbTe
Dimension	56 mm x 56 mm
Hot side temperature	350°C
Cold side temperature	30°C
Open Circuit Voltage	9.2 V
Matched Load Resistance	$0.97\ \Omega$
Matched Load output Voltage	4.6 V
Matched Load output Current	4.7 A
Matched Load output Power	21.7 W
Heat flow across the module	$\approx 310\ \text{W}$
Heat flow density	$\approx 9.88\ \text{W/cm}^2$
AC resistance measured under 27°C @ 1000 Hz	$0.42 \sim 0.52$

The micro T-type thermocouple can measure upto a temperature of 350°C with an uncertainty of $0.5^\circ\text{C} \pm 0.14\%$ and a dimension of 0.5mm diameter. The details of thermocouple positioning are given in Table 5. The entire TEG unit is insulated using ceramic wool. A varying external load (0 - $2\ \Omega$) is connected to the hybrid TEG and the corresponding voltage and current values at different resistance values are measured using a digital voltmeter (DROK 090514) and ammeter (DROK 090828) respectively. A data acquisition (Agilent 34972 A) unit

is used to record the necessary vital data for additional processing. Laboratory based experiments are carried out and the corresponding findings are noted.

Table 5. Thermocouple positioning

Thermocouple	Position	Measurement (°C)
T ₁	Hot side copper block	Heater temperature
T ₂	Between copper block and hot side of TEG	Hot side temperature
T ₃	Between cold side of TEG and copper block	Cold side temperature
T ₄	Water inlet port	Inlet water temperature
T ₅	Water outlet port	Outlet water temperature

WATER-COOLING TECHNIQUE

In water cooling method – forced convection method, water is being used as the coolant. A hollow copper block filled with water is fixed to the cold side of the hybrid *TEG* to remove the residual heat energy. A constant temperature bath is used to maintain the coolant water temperature at 30°C. The flow rate of the coolant was controlled using a flow control valve. The flow rates are measured by direct weighing of the fluid (100ml). The time measurements were repeated for more than ten times and the average value was considered and the measuring error of the flow rate was found to be less than 1.5%. The flow rate of the coolant is fixed at 0.5l/min using a flow control valve [36]. The test-section of the hybrid *TEG* with water as the coolant is shown in Figure 5a.

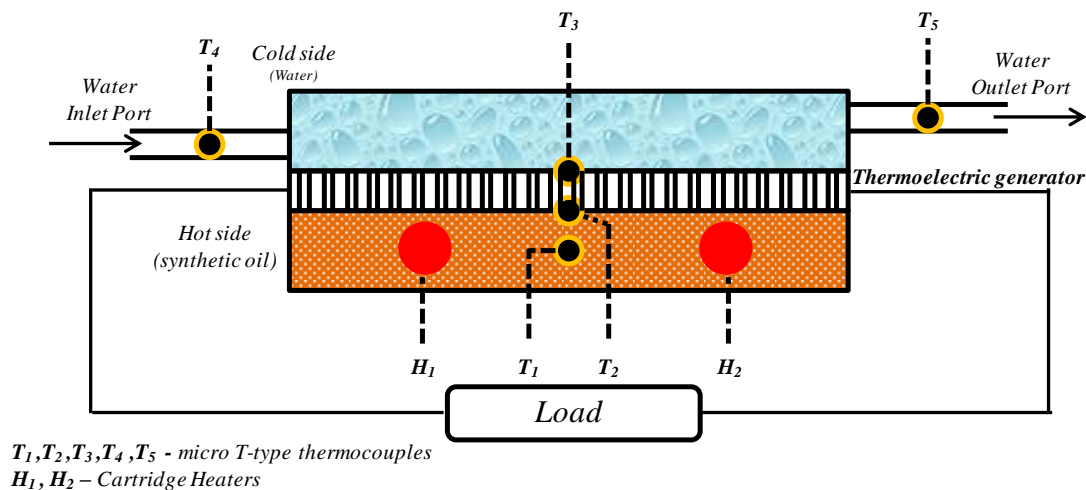


Figure 5a. Test section – forced convection

The water flow loop heat exchanger is a hollow copper block with a single inlet and outlet port. Water is being used as a coolant and the inlet water temperature is being maintained at 30°C using a constant temperature bath. Water flows inside the hollow copper block placed above the cold side of hybrid *TEG* through the inlet port and leaves the hollow copper block through the outlet port. The micro T-type thermocouple is placed exactly at about 28mm from either side of the hybrid *TEG*, over the cold side to measure the cold side temperature. In addition, two thermocouples, one at the inlet side and the other at the outlet side are placed to measure the water inlet and outlet temperature. In the same manner, thermocouple was placed over the hot side of the hybrid *TEG*. Since it is a single module performance analysis, only a single thermocouple is used to measure the relevant cold side temperature. The hot side and cold side temperatures are monitored using the DAQ (Agilent 34972 A) unit.

AIR-COOLING TECHNIQUE

In air cooled method – natural convection method, a copper block with small fins is attached to the cold side of the hybrid *TEG*. The copper block with small fins used in natural convection air-cooling system has been designed inhouse. A 60 mm x 60mm solid copper block is taken and copper has been **extruded or skived** using sharp and accurately controlled blade such that the fin thickness is about 4 mm and length is about 20mm with 8 fins. The cold side of the hybrid *TEG* is maintained at ambient conditions (around 30 °C). The test-section of the hybrid *TEG* with natural convection air cooling method is shown in Figure 5b.

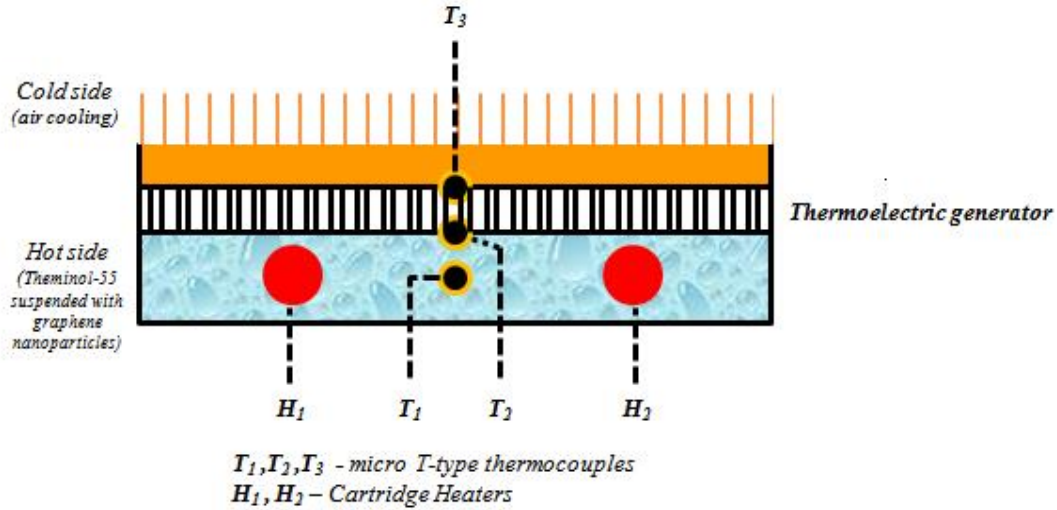


Figure 5b. Test section – natural convection

DATA REDUCTION

The output power, P is the product of output voltage and current; it is calculated as given in Equation 1

$$P = V \times I \quad (1)$$

where, V is the measured output voltage, I is the measured output current.

Maximum power output is attained when the internal resistance of the hybrid TEG (R_i) matches with the externally connected load resistance (R_L). This is termed as the matched load resistance (R_{mL}). The maximum power output is calculated using Equation 2,

$$P_{\max} = \frac{\alpha^2 \Delta T^2}{4R_{mL}} \quad (2)$$

where, α is the seebeck co-efficient defined as the ratio of the open circuit voltage, V_{oc} to the temperature gradient across the hot and cold sides of the hybrid TEG, $\Delta T = T_H - T_C$ as given in Equation 3.

$$\alpha = \frac{V_{oc}}{\Delta T} \quad (3)$$

The thermoelectric generator efficiency is calculated using the relation given in equation 4 as follows,

$$\eta = \frac{P}{Q} \quad (4)$$

where, P is the output power of the hybrid TEG obtained as in Equation 1; Q is the heat input to the system and can be calculated as given in Equation 5.

$$Q = K_m (T_H - T_C) + \alpha I T_H - \frac{I^2 R_i}{2} \quad (5)$$

where, α is the Seebeck co-efficient calculated as in Equation 3, K_m is the thermal conductance R_i is the internal resistance of the TEG module and calculated as in Equation 6 and 7 [37].

$$K_m = \frac{(T_H - \Delta T_{\max}) V_{\max} I_{\max}}{2T_H \Delta T_{\max}} \quad (6)$$

$$R_i = R_L \left(\frac{V_{OC}}{V} - 1 \right) \quad (7)$$

where, R_L is the load resistance, V_{OC} is the open circuit voltage and V is the measured load voltage.

UNCERTAINTY ANALYSIS

Type A Uncertainty Analysis

Type A analysis involves calculation of uncertainties based on statistical analysis of data such as random errors, repeatability test, bias and so on. An error analysis for hot side temperature of 250°C and a flow rate of 0.5 l/min under both water and air cooled techniques is done and the uncertainty values are given in Table 6. Measurement has been taken for approximately 15 data sets but only 3 data sets are shown for reference. For each individual quantity, the mean and standard deviation values are obtained using the following equations 8,9 and 10 [38].

$$\bar{X} = \frac{1}{n} \sum_{i=1}^n X_i \quad (8)$$

$$SD = \left[\frac{1}{n-1} \sum_{i=1}^n (X_i - \bar{X})^2 \right]^{1/2} \quad (9)$$

The uncertainty is given by,
$$U\% = \left(\frac{SD}{\bar{X}} \right) \times 100 \quad (10)$$

The uncertainty in the hot side temperature on the basis of repeatability test is found to be around 0.13% and in cold side, it was found to be 1.15% for water cooled technique and 0.77% for air-cooled method. The uncertainties based on Type A Evaluation technique is tabulated in Table 6.

Table 6. Type A Uncertainty Analysis

Method	Variable	I	II	III	Mean	SD	Uncertainty	U%
	T_H (°C)	250.07	250.68	250.51	250.42	0.314802	0.001257	0.13
Water cooled	flow rate (mins)	3.29	3.25	3.34	3.293333	0.045092	0.013692	1.4
	T_C (°C)	50.63	49.48	50.05	50.05364	0.57547	0.011497	1.15
	ΔT (°C)	199.37	200.52	199.95	199.9464	0.57547	0.002878	0.29
	V_{oc} (V)	3.82	3.79	3.84	3.816667	0.025166	0.006593	0.66
	P_{\max} (W)	6.51	6.47	6.54	6.506667	0.035119	0.005397	0.54
Air cooled	T_C (°C)	70.15	70.83	69.77	70.25	0.537029	0.007644	0.77
	ΔT (°C)	179.85	179.17	180.23	179.75	0.537029	0.002987	0.3
	V_{oc} (V)	3.38	3.34	3.28	3.3333	0.050332	0.0151	1.68
	P_{\max} (W)	5.06	5.19	5.11	5.12	0.065574	0.012807	1.28

The uncertainty in power is calculated based on scientific judgment using all of the significant information included in manufacturer's specification. Power is calculated by multiplying measured voltage and current as given in Equation 1. Hence the uncertainties in voltage and current measurement affect the measured output power to some extent. The uncertainty of maximum output power based on voltage and current values measured using voltmeter and ammeter and their uncertainties is calculated using equation 11 [38],

$$U_p = \sqrt{\left(\frac{\partial V}{V}\right)^2 u_v^2 + \left(\frac{\partial I}{I}\right)^2 u_i^2} \quad (11)$$

where, $\frac{\partial V}{V}$ and $\frac{\partial I}{I}$ are the voltage and current values measured using voltmeter and ammeter respectively; u_v and u_i are the uncertainties of voltmeter and ammeter respectively. For water-cooled technique, uncertainty of maximum output power is calculated as $\sqrt{(1.62)^2 (0.01)^2 + (4.04)^2 (0.01)^2} = \pm 4.35\%$. For air-cooled technique, uncertainty of maximum output power is calculated as $\sqrt{(1.91)^2 (0.01)^2 + (2.65)^2 (0.01)^2} = \pm 2.9\%$.

Type B Uncertainty Analysis

Before conducting experiments, the instruments are calibrated in order to resolve the uncertainties. The uncertainties associated with instrument calibration are reported in Type B Evaluation. The instruments, their operating range and percentage uncertainty values as reported in instruments instruction manual are listed in Table 7. The relative standard uncertainty of the power can be calculated using equation 12.

$$U_{p, std} = \frac{1}{\sqrt{3}} \sqrt{u_v^2 + u_i^2} = U_{p, std} = \frac{1}{\sqrt{3}} \sqrt{0.01^2 + 0.001^2} = 1.41\% \quad (12)$$

where, u_v and u_i are the worst case relative uncertainties of voltmeter and ammeter; the co-efficient $\frac{1}{\sqrt{3}}$ is used to convert the worst case uncertainty to standard uncertainty. The relative standard uncertainty of power based on the measuring equipments is found to be 0.082%.

Table 7. List of Equipment Uncertainty

Equipment	Operating Range	Uncertainty
T-type thermocouple	Upto 350 °C	0.5°C ± 0.14%
Heater	Upto 400 °C	0.1°C ± 0.02%
Flow meter	0.5 to 1.5 lit/min	0.01 lit/min ± 0.7%
Voltmeter	0 to 10 V	0.01 V ± 0.1%
Ammeter	0 to 9.99 A	0.01 A ± 2%

An uncertainty calculation that takes into account both repeatability errors and systematic effects is done by taking the root sum of squares of both Type A and Type B relative standard uncertainties. The combined uncertainty in maximum power output under water-cooled technique is found to be, $U_{com_w} = \sqrt{0.0435^2 + 0.0141^2} = \pm 4.35\%$. Similarly, the combined uncertainty in maximum power output under air-cooled technique is found to be, $U_{com_a} = \sqrt{0.029^2 + 0.0141^2} = \pm 3.2\%$.

ARTIFICIAL NEURAL NETWORKS

The Backpropagation neural network is a multilayered, feedforward neural network that is most commonly used for supervised training of artificial neural networks. Selection of proper architecture plays an important role in predicting the classification accuracy. In the present work, a three layered network – an input layer, one hidden layer and an output layer is developed. For each input vector, a desired output is required. The proposed structure of ANN is shown in Figure 5.

Initially, one input value is propagated forward through the ANN, layer-by-layer, until it reaches the output layer. The computed output vector is then compared with the required desired output to determine the errors. These errors are propagated backwards from the output layer to the input layer through the ANN. The above process is repeated either till the desired output is reached or till the errors are minimized. There are quite a lot of

training algorithms available for feed forward networks. These training algorithms use the gradient of performance function to determine the bias correction term and adjust the network weights in the direction in which the performance minimizes at faster rate. The gradient is found using a technique called back propagation in which the computation is carried out backwards through the network.

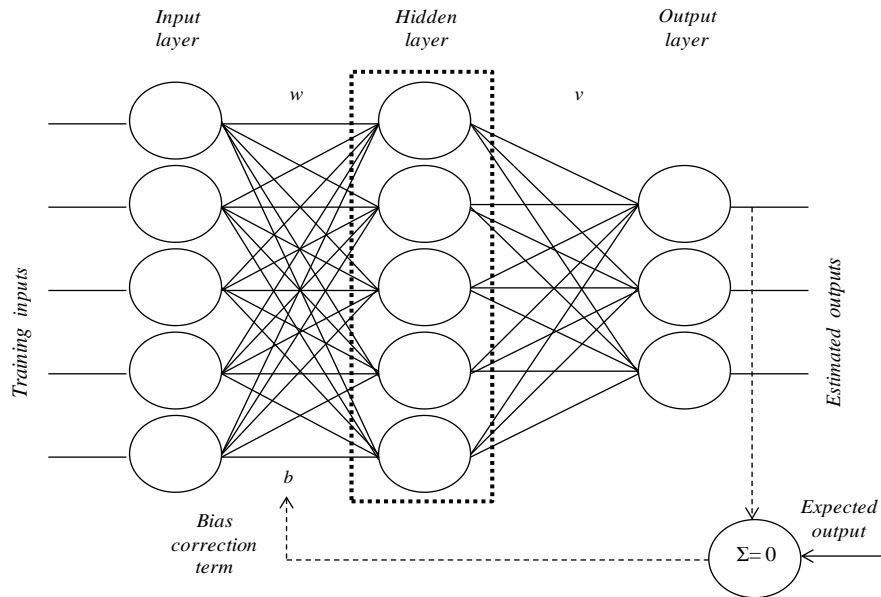


Figure 6. Proposed structure of ANN

RESULTS AND DISCUSSION

The temporal-temperature distribution of the hot (T_H) end at an input temperature of 250°C and the obtained temperature gradient using water and air cooling techniques is shown in Figure 7. On practical application, it was seen that the difference between the heater temperature and the hot side temperature ($T_h \sim T_H$) of the hybrid *TEG* module was found to be below 1°C . The variation in temperature is very small and insignificant. Hence, the heater temperature and hot side temperature is considered to be approximately the same ($T_h \approx T_H$). From Figure 7, it is observed that the hot side temperature of the hybrid *TEG* module increases swiftly upto 240°C in 11.20 minutes. At about 23.34 minutes, the hot side temperature almost reaches steady state and the graph becoming almost straight.

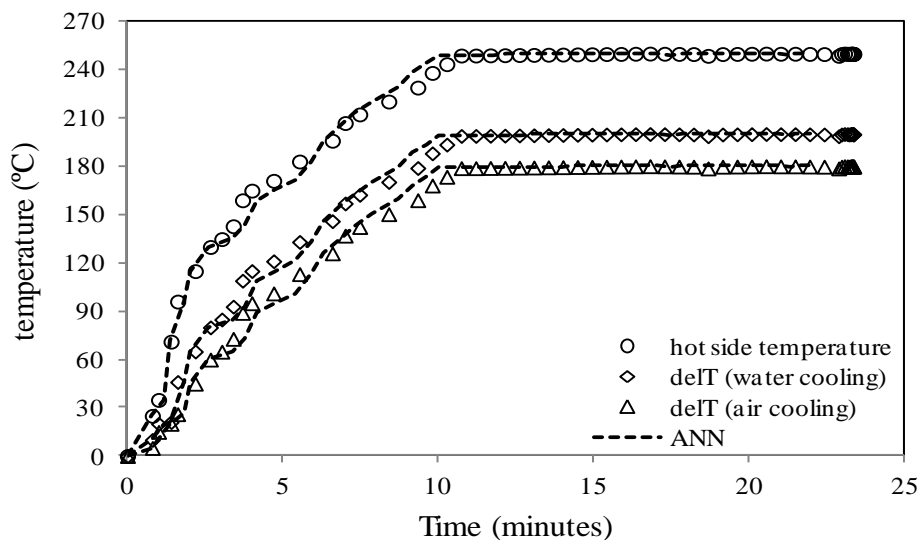


Figure 7. Variation in temperature with time

Experiments have been performed for a hot side temperature range of 200 - 250°C. But, only a sample result for 250°C hot side temperature is shown for reference. The water temperature on the cold side was maintained constant at 30°C using a constant temperature bath throughout the practical implementation. Evaluation of ANN data based on sample data is done to prove the closeness between both the techniques. Depending on the acquired accurate results, performance of hybrid *TEG* is estimated beyond 250°C hot side temperature with a temperature difference of 200°C for water cooling method and 180°C for air cooling method. The heater input temperature is varied from 200 - 250°C with the coolant temperature being maintained at 30°C. A flow rate of 0.5 l/min was fixed for the coolant in water cooled technique [36]. Sample experimental values are noted down. The obtained experimental data is utilized to train the ANN network and based on the obtained results; the closeness between both the methodologies is checked and proved.

Using the sample experimental data, the ANN was trained and it was found that the hot side temperature reached steady state in about 22.86 minutes, which is more or less similar to outcome of experimental approach. The variation between the experimental method and ANN based approach is about 0.48 minutes. This shows the proximity or closeness between both the methodologies. Thus, it can be confirmed that ANN approach can give excellent outcome without the need of carrying out experiments.

Now, a 0 - 2 Ω load resistance is externally connected to the hybrid *TEG* module. The load resistance, R_L is divided into 14 identically spaced markings with a resistance change step of 0.14Ω. At each resistance marking, the corresponding values of current and voltage are noted and the output power is calculated. The output power as a function of load resistance is given in Figure 8.

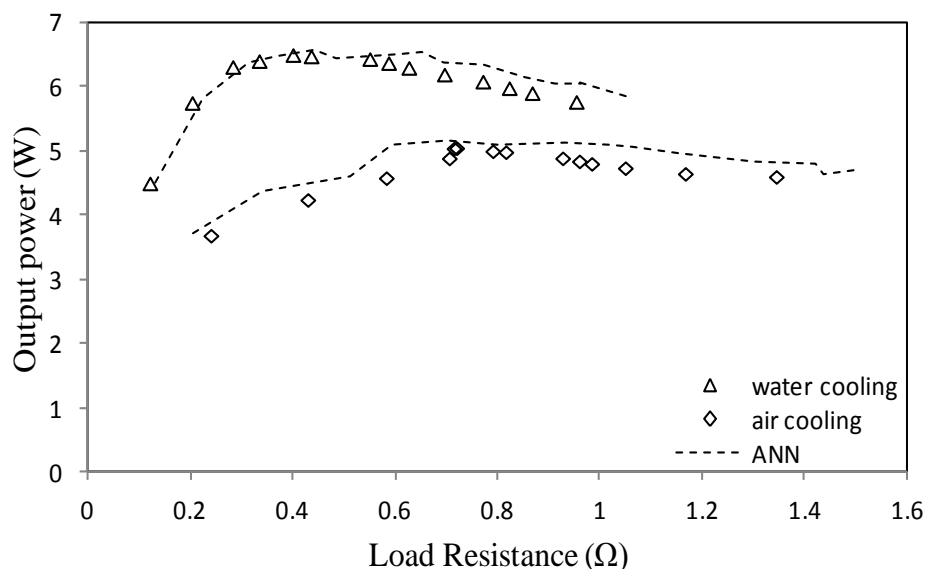


Figure 8. Variation of output power with load resistance

At a hot side temperature of 250°C, under water cooling technique, the cold side temperature (T_3) was found to be around 50°C and the maximum power obtained was found to be 6.51W at a matched load resistance of 0.3994Ω. In air cooled technique, the cold side temperature (T_3) was found to be around 70°C and the maximum power was found to be 5.06W at a matched load resistance of 0.719Ω. At the same hot side temperature, the cold side temperature (T_3) for both water and air-cooled methods was found to vary and was less for water-cooled technique because due to forced convection of water, the heat transfer rate was found to be more in water-cooled method than the natural convection of air. When simulated using ANN, under water cooled technique, the maximum power obtained was found to be 6.56W and under air cooled technique, the maximum power was found to be 5.17W. The variation in results obtained from both the methodologies is about 0.05W and 0.11W which is more or less negligible and shows the proximity or nearness between both the approaches.

Figure 9 shows the performance (electrical characterization) curve when the hybrid *TEG* operates at hot side temperature of 250°C under water and air cooled conditions.

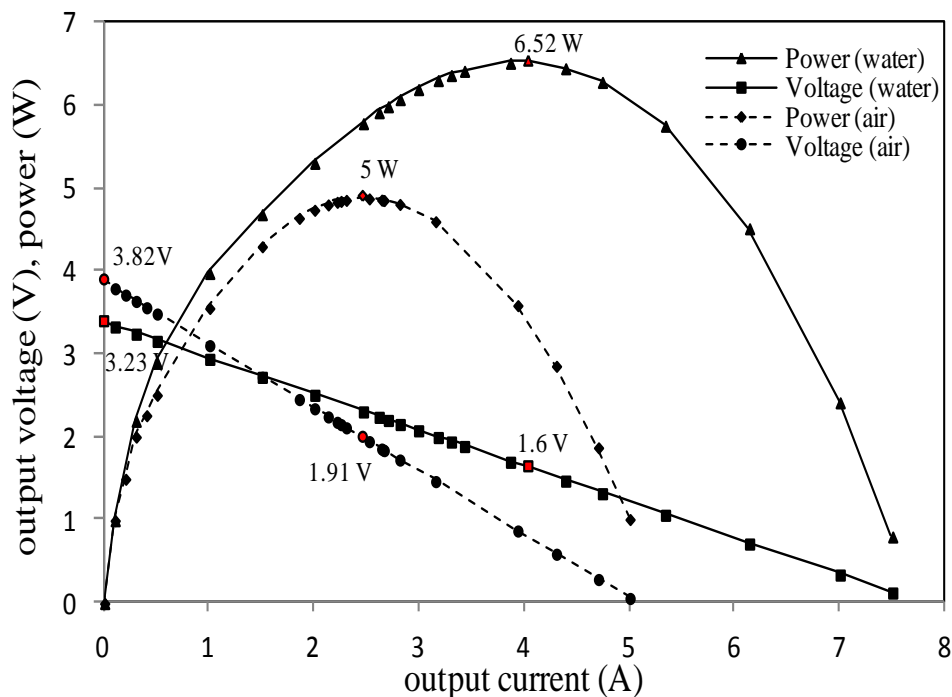


Figure 9. Electrical characterization at $T_H = 250^\circ\text{C}$ – water cooling & air cooling

The straight line represents the voltage-current (V-I) characteristics and the curved line represents the power-current (P-I) characteristics of the *TE* device. The open-circuit voltage (V_{OC}) is the voltage at which the *TEG* terminals are open-circuited and no current is drawn by the load resistance. The short-circuit current (I_{SC}) is the current obtained when the *TEG* terminals are short-circuited. The maximum power is obtained when $V_L = V_{OC}/2$ and $I_L = I_{SC}/2$ and at matched load resistance – the resistance value at which the externally connected load resistance (R_L) and the internal resistance (R_i) of the *TEG* are equal. Initially, when the *TEG* operates till the maximum power point, less current flows through the thermoelectric device and as the current increases, Peltier effect becomes prevalent due to which the thermal conductivity of the device is lesser than the energy that flows at maximum power point. Hence a lower thermal load is imposed on the system leading to increased thermal system efficiency. After the maximum power point, thermal conductivity of the device increases and is greater than the energy that flows at maximum power point leading to decreased thermal system efficiency. At a hot side temperature of 250°C , the maximum power obtained under water cooled condition is about 6.52W and 5W under air cooled condition.

Figure 10 gives the relation between the efficiency of the system and the load resistance. From Figure 10, it is evident that the efficiency of the system increases till the maximum power point and then decreases beyond the maximum power point. This variation in system efficiency depends mainly on the energy that flows at the maximum power point. At a hot side temperature of 250°C , when the load resistance is increased from $0 - 2\Omega$, under water cooled technique, the efficiency was found to vary from 1.29% to 1.65% and under air cooled technique, the efficiency was found to vary from 1.05% to 1.31%. When simulated using ANN, under water cooled technique, the efficiency was found to be varying from 1.29% to 1.66% and under air cooled technique, the efficiency was found to vary from 1.06% to 1.34%. It was observed that the experimentally measured values of open circuit voltage and the values obtained by ANN based approach were almost similar. The variation between both the approaches was found to be in the range of $0 - 0.02\%$ for water cooled method and $0.01 - 0.03\%$ for air cooled method which is purely negligible and also shows the proximity between both the approaches.

The open circuit voltage is measured for different hot side temperatures ranging from $200 - 250^\circ\text{C}$, at a fixed coolant temperature. For various hot side temperatures, the open circuit voltage is measured by disconnecting the externally connected load across the hybrid *TEG*.

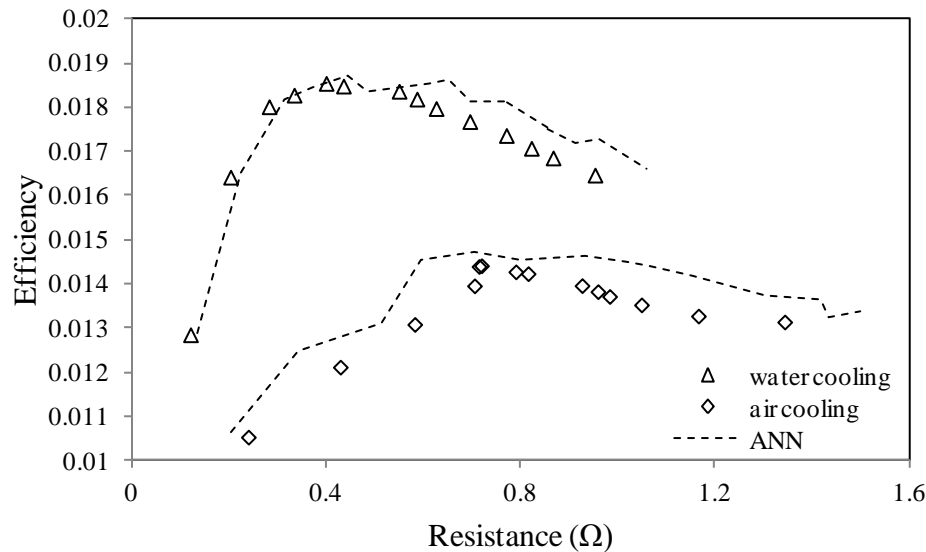


Figure 10. Variation in efficiency with respect to load resistance.

The variation in the open circuit voltage with respect to the hot side temperature under water and air cooled methods is shown in Figure 11. At a hot side temperature range of 200 - 250°C, under water cooled technique, the open circuit voltage was found to vary from 2.42V to 3.38V and under air cooled technique, the open circuit voltage was found to vary from 2.75V to 3.81V. When simulated using ANN, under water cooled technique, the open circuit voltage was found to be varying from 2.48V to 3.34V and under air cooled technique, the open circuit voltage was found to vary from 2.78V to 3.85 V. It was observed that the experimentally measured values of open circuit voltage and the values obtained by ANN based approach were almost similar. The variation between both the approaches was found to be in the range of 0.04V to 0.06V for water cooled method and 0.03V to 0.04V for air cooled method which is purely negligible and also shows the proximity between both the approaches.

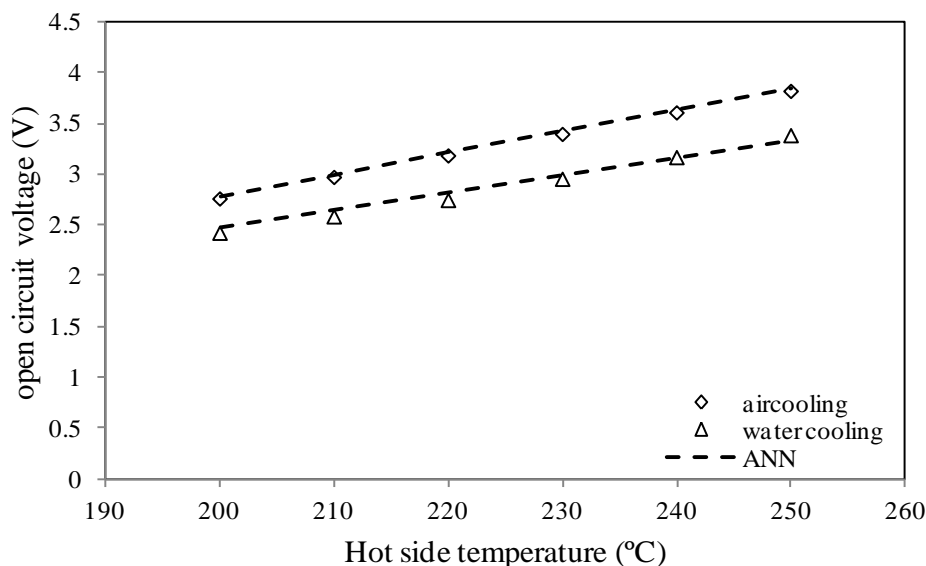


Figure 11. Variation in open circuit voltage with hot side temperature

Similarly, the maximum output power is measured for different hot side temperatures ranging from 200 - 250°C. The maximum output power is measured by disconnecting the externally connected load across the hybrid TEG. Figure 12 shows the variation in the maximum power output with respect to the temperature gradients under water and air cooled methods as shown if. At a hot side temperature range of 200 - 250°C, under water cooled technique, the maximum output power was found to vary from 5W to 6.67W and under air cooled technique, the

maximum output power was found to vary from 3.81W to 5.27W. When simulated using ANN, under water cooled technique, the maximum output power was found to be varying from 4.88W to 6.5W and under air cooled technique, the maximum output power was found to vary from 3.66W to 5.06W. It was observed that the experimentally measured values of maximum power output and the values obtained by ANN based approach were almost similar. The variation between both the approaches was found to be in the range of 0.15W to 0.21W for water cooled method and 0.12W to 0.16W for air cooled method which is almost equal and also shows the proximity or nearness between both the approaches.

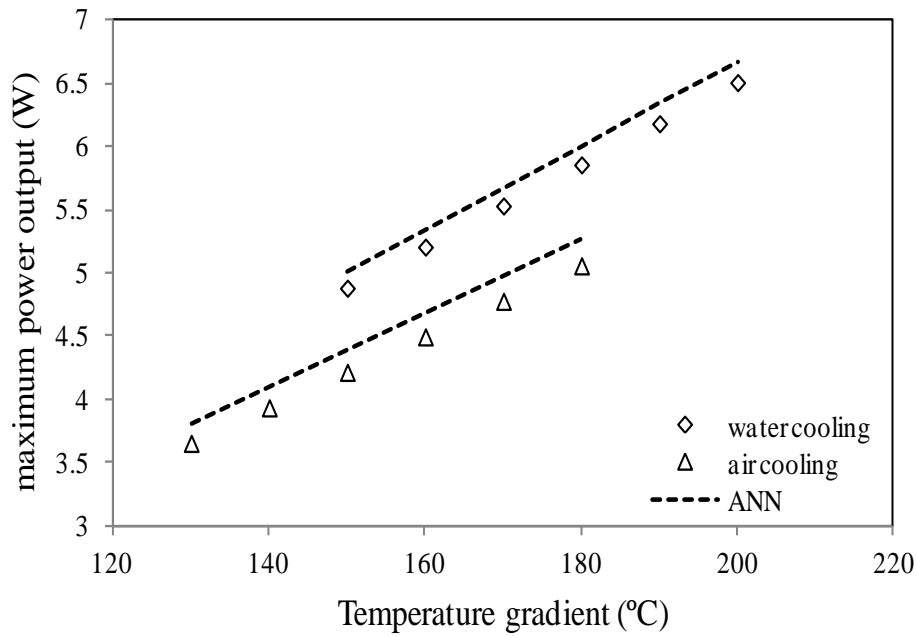


Figure 12. Variation in maximum output power with temperature difference

The matched load resistance is measured for different hot side temperatures ranging from 200 - 250°C. Matched load resistance is the resistance value at which the internal resistance of the *TEG* matches with the externally connected load resistance. Also, maximum power output occurs at matched load resistance. Figure 13 shows the variation in the matched load resistance with respect to the temperature gradients under water and air cooled methods as shown in. At a hot side temperature range of 200 - 250°C, under water cooled technique, the matched load resistance was found to vary from 0.299Ω to 0.399Ω and under air cooled technique, the matched load resistance was found to vary from 0.52Ω to 0.72Ω. When simulated using ANN, under water cooled technique, the matched load resistance was found to be varying from 0.33Ω to 0.44Ω. and under air cooled technique, the matched load resistance was found to vary from 0.55Ω to 0.74Ω. It was observed that the experimentally measured values of matched load resistance and the values obtained by ANN based approach were almost similar. The variation between both the approaches was found to be in the range of 0.031Ω to 0.045Ω, for water cooled method and 0.02Ω to 0.03Ω, for air cooled method which is almost equal and also shows the proximity or nearness between both the approaches.

From Figures 7 to 13, it can be concluded that both the performance of ANN based approach and experimental method is comparable. This proves that ANN provides precise results even without the need of performing experiments. Hence, performance parameters such as open circuit voltage and maximum output power can be estimated using ANN which is shown in the consequent results. Thus, it can be confirmed that ANN approach can give excellent outcome for hot side temperatures beyond 250°C without the need of carrying out experiments.

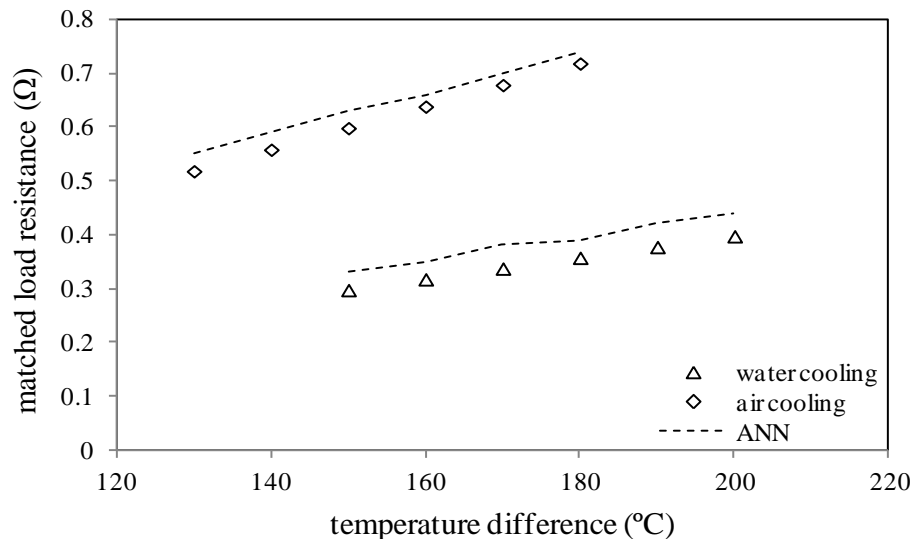


Figure 13 Variation in matched load resistance with temperature difference

Table 8. Estimation of Open circuit voltage and maximum power output at different temperature gradients – water cooling

Temperature gradient (ΔT) in $^{\circ}\text{C}$	Open circuit voltage (V_{oc}) in V		Maximum Power output (P_{max}) in W		Matched Load Resistance (R_{mL}) in Ω	
	Experimental Approach	ANN Approach	Experimental Approach	ANN Approach	Experimental Approach	ANN Approach
150	2.419	2.48	4.883	5	0.299	0.33
160	2.58	2.65	5.208	5.33	0.320	0.35
170	2.741	2.82	5.534	5.67	0.339	0.38
180	2.95	2.99	5.859	6	0.359	0.39
190	3.164	3.16	6.185	6.33	0.379	0.42
200	3.38	3.34	6.51	6.67	0.399	0.44
230	-	3.84	-	7.76	-	0.51
260	-	4.62	-	8.63	-	0.58
290	-	4.87	-	9.75	-	0.64
320	-	5.44	-	10.72	-	0.71

The variations in open circuit voltage, maximum output power and matched load resistance with respect to the various temperature gradients under water cooled and air cooled techniques are shown in are shown in Tables 8 and 9.

Table 9. Estimation of Open circuit voltage and maximum power output at different temperature gradients – air cooling

Temperature gradient (ΔT) in $^{\circ}\text{C}$	Open circuit voltage (V_{oc}) in V		Maximum Power output (P_{max}) in W		Matched Load Resistance (R_{mL}) in Ω	
	Experimental Approach	ANN Approach	Experimental Approach	ANN Approach	Experimental Approach	ANN Approach
130	2.756	2.78	3.655	3.81	0.52	0.55
140	2.968	2.99	3.936	4.09	0.56	0.59
150	3.18	3.21	4.217	4.39	0.6	0.63
160	3.392	3.43	4.498	4.68	0.64	0.66
170	3.604	3.64	4.779	4.97	0.68	0.70
180	3.816	3.85	5.06	5.27	0.72	0.74
200	-	4.28	-	5.86	-	0.86
230	-	4.92	-	6.73	-	0.98
260	-	5.56	-	7.61	-	1.02
290	-	6.20	-	8.49	-	1.14
300	-	6.41	-	8.78	-	1.18

COST ANALYSIS

The unit cost of the hybrid thermoelectric module *TEG1-PB-12611-6.0*, supplied by Thermal Electronics Corporation, Canada, used in the current study, is about \$69. The unit cost is further reduced to \$7 when the quantity is increased to a higher number (~10,000 units). Initial investment cost of setting up a biomass gasification plant is about \$1500 [39]. The solid residue that is left after removal of oil from the non-edible *Pongamia Pinnata* seed is *Pongamia de-oiled seed cake*, also termed as Biomass waste; is gasified, combusted and used as input heat source to the thermoelectric generator. Since the disposal of de-oiled *Pongamia* seed cake is of huge concern, while evaluating the cost of power generated from Biomass gasified-thermoelectric system, the fuel cost is considered to be negligible/zero. The simplified levelized cost of electricity, *sLCOE* is the ratio of the total annual cost to the total amount of electricity generation and is mathematically expressed as in Equation 9 [40].

$$sLCOE = \frac{(CC \times CRF) + fixO \& MC}{365 \times 24 \times CF \times systemcapacity} + (FC \times heatrate) + var O \& MC \quad (9)$$

where, *CC* is the capital cost (includes cost of the modules, heat sink, cooling system, electronic control system), *CF* is the capacity factor, *FC* is the fuel cost and *CRF* is the capital recovery factor and is calculated using Equation 10.

$$CRF = \frac{d(1+i)^t}{(1+d)^t - 1} \quad (10)$$

where, *d* is the decimal interest rate and *t* is the number of years of repayment of loan. If a 5 year loan at an interest rate of 4% is assumed, the *CRF* is calculated using Equation 10 and is found to be 0.2246. The fixed Operation and Maintenance cost (*fixO&MC*) is found to be either 3% or 6% of the annual capital cost [41]. The variable Operation and Maintenance cost (*varO&MC*) is found to be \$3.7/MW hr [41]. Based on the above mentioned data and using equation 9, the cost of Biomass gasified-thermoelectric system is estimated to be \$0.0018/kW h and in terms of Indian currency is rupees 0.0676/kWh. Hence, it can be concluded that the power generated using thermoelectric generators is almost negligible when compared with that of the other renewable energy resources. Similar analysis has also been reported by Seijiro et al [42] and found that the cost involved in using *TEG* technology for power generation is negligible. Table 10 gives the list of electric power generation cost of various generating methods.

CONCLUSIONS

Based on the current study, the following conclusions are drawn:

- i. Proximate and Ultimate analysis of *Pongamia de-oiled seed cake* showed the presence of high amount of carbon content. Gasification of *Pongamia de-oiled seed cake* resulted in a “Syngas” and on combustion produced higher energy biomass waste heat with a temperature of about 250 - 350°C.
- ii. Results showed that an enhancement in electric power of 22.27% is obtained when water is used on the cold side of the *TEG* at a constant hot side temperature of 250°C.
- iii. By using ANN based approach, the open circuit voltage and maximum power output for hot side temperatures beyond 250°C is estimated using ANN based approach for water and air cooled conditions. At a hot side temperature of 350°C, the open circuit voltage under water and air cooled techniques were estimated to be 5.44V and 6.84V respectively. Similarly, the maximum output power under water and air cooled techniques were estimated to be 10.72W and 8.78W respectively at a matched load resistance of 0.71Ω and 1.21Ω.
- iv. Cost of Biomass gasified-thermoelectric system is estimated to be \$0.0018/kWh and in terms of Indian currency is rupees 0.0676/kWh, which is almost negligible when compared with other renewable energy technologies.

NOMENCLATURE

<i>sLCOE</i>	simplified levelized cost of electricity (cost/kWh)
<i>CC</i>	capital cost
<i>CF</i>	capacity factor
<i>CRF</i>	capital recovery factor
<i>FC</i>	fuel cost
<i>d</i>	decimal interest rate (%)
<i>t</i>	loan repayment time (years)
<i>I</i>	current (A)
<i>K</i>	thermal conductance (W/K)
<i>P</i>	output power (W)
<i>Q</i>	heat input (W)
<i>R</i>	resistance (Ω)
<i>T</i>	temperature ($^{\circ}C$ or K)
<i>U</i>	uncertainty (%)
<i>V</i>	voltage (V)
<i>α</i>	seebeck co-efficient (V/K)
<i>η</i>	efficiency (%)
<i>ΔT</i>	TEG hot side to cold side temperature difference ($^{\circ}C$ or K)
<i>a</i>	air
<i>com</i>	combined
<i>h</i>	heater
<i>i</i>	internal
<i>max</i>	maximum of given quantity
<i>mL</i>	matched load
<i>oc</i>	open circuit
<i>w</i>	water
<i>w1</i>	water inlet
<i>w2</i>	water outlet
<i>C</i>	TEG cold side
<i>H</i>	TEG hot side
<i>L</i>	load

CONFLICT OF INTEREST

The authors confirm that this article content has no conflict of interest among the authors.

ACKNOWLEDGEMENT

The first, second and third authors gratefully acknowledge the financial support provided by the funding agency, the Department of Science and Technology (DST), Science and Engineering Research Board (SERB), (SB/FTP/ETA-362/2012), New Delhi, India. The fourth author acknowledges the support provided by the "Research Chair Grant" National Science and Technology Development Agency (NSTDA), the Thailand Research Fund (TRF), the National Research University Project (NRU) and King Mongkut's University of Technology Thonburi through the "KMUTT 55th Anniversary Commemorative Fund". The authors would like to thank Mr. Jaya Seelan R of Karunya University for helping in the fabrication of the experimental test facility.

REFERENCES

- [1] Prakash, R., Christopher, D., & Kumarrathinam, K. (2015). Analysis of Surface Waste Heat Recovery in IC Engine by Using TEG. In Applied Mechanics and Materials (Vol. 787, pp. 782-786). Trans Tech Publications.
- [2] Liu, X., Deng, Y. D., Li, Z., & Su, C. Q. (2015). Performance analysis of a waste heat recovery thermoelectric generation system for automotive application. Energy Conversion and Management, 90, 121-127.
- [3] Chandi, R. M., & Rajeev, R. (2015). Design and Analysis of Heat Exchanger for Automotive Exhaust based Thermoelectric Generator [TEG]. International Journal for Innovative Research in Science & Technology, 1(11).
- [4] Deok In, B., ik Kim, H., wook Son, J., & hyung Lee, K. (2015). The study of a thermoelectric generator with various thermal conditions of exhaust gas from a diesel engine. International Journal of Heat and Mass Transfer, 86, 667-680.
- [5] Liu, C., & Li, W. Z. (2015). An Experimental Study of a Two-stage Thermoelectric Generator Using Heat Pipe in Vehicle Exhaust. Distributed Generation and Alternative Energy Journal, 30(1), 15-37.
- [6] Liu, Z., Zhang, L., Gong, G., Luo, Y., & Meng, F. (2015). Evaluation of a prototype active solar thermoelectric radiant wall system in winter conditions. Applied Thermal Engineering, 89, 36-43.

- [7] Alomair, Y., Alomair, M., Mahmud, S., & Abdullah, H. A. (2015). Theoretical and experimental analyses of solar-thermoelectric liquid-chiller system. *International Journal of Refrigeration*, 56, 126-139.
- [8] Liu, Z., Zhang, L., Gong, G., & Han, T. (2015). Experimental evaluation of an active solar thermoelectric radiant wall system. *Energy Conversion and Management*, 94, 253-260.
- [9] Özdemir, A. E., Köysal, Y., Özbaş, E., & Atalay, T. (2015). The experimental design of solar heating thermoelectric generator with wind cooling chimney. *Energy Conversion and Management*, 98, 127-133.
- [10] Liu, Z., Zhang, L., & Gong, G. (2014). Experimental evaluation of a solar thermoelectric cooled ceiling combined with displacement ventilation system. *Energy Conversion and Management*, 87, 559-565.
- [11] Killander, A., & Bass, J. C. (1996, March). A stove-top generator for cold areas. In *Thermoelectrics, 1996., Fifteenth International Conference on* (pp. 390-393).
- [12] O'Shaughnessy, S. M., Deasy, M. J., Kinsella, C. E., Doyle, J. V., & Robinson, A. J. (2013). Small scale electricity generation from a portable biomass cookstove: prototype design and preliminary results. *Applied Energy*, 102, 374-385.
- [13] Champier, D., Bedecarrats, J. P., Rivaletto, M., & Strub, F. (2010). Thermoelectric power generation from biomass cook stoves. *Energy*, 35(2), 935-942.
- [14] Nuwayhid, R. Y., Shihadeh, A., & Ghaddar, N. (2005). Development and testing of a domestic woodstove thermoelectric generator with natural convection cooling. *Energy Conversion and Management*, 46(9-10), 1631-1643.
- [15] Lertsatitthanakorn, C. (2007). Electrical performance analysis and economic evaluation of combined biomass cook stove thermoelectric (BITE) generator. *Bioresource technology*, 98(8), 1670-1674.
- [16] Jayakumar, J. (2015, March). Analysis of (Bi₂Te₃-PbTe) hybrid thermoelectric generator for effective power generation. In *Innovations in Information, Embedded and Communication Systems (ICIIECS), 2015 International Conference on* (pp. 1-6).
- [17] Elghool, A., Basrawi, F., Ibrahim, T. K., Habib, K., Ibrahim, H., & Idris, D. M. N. D. (2017). A review on heat sink for thermo-electric power generation: Classifications and parameters affecting performance. *Energy conversion and management*, 134, 260-277.
- [18] O'Shaughnessy, S. M., Deasy, M. J., Doyle, J. V., & Robinson, A. J. (2014). Field trial testing of an electricity-producing portable biomass cooking stove in rural Malawi. *Energy for Sustainable development*, 20, 1-10.
- [19] Montecucco, A., Siviter, J., & Knox, A. R. (2017). Combined heat and power system for stoves with thermoelectric generators. *Applied Energy*, 185, 1336-1342.
- [20] O'Shaughnessy, S. M., Deasy, M. J., Doyle, J. V., & Robinson, A. J. (2015). Adaptive design of a prototype electricity-producing biomass cooking stove. *Energy for sustainable development*, 28, 41-51.
- [21] Montecucco, A., Siviter, J., & Knox, A. R. (2015). A combined heat and power system for solid-fuel stoves using thermoelectric generators. *Energy Procedia*, 75, 597-602.
- [22] Mal, R., Prasad, R., & Vijay, V. K. (2016). Multi-functionality clean biomass cookstove for off-grid areas. *Process Safety and Environmental Protection*, 104, 85-94.
- [23] O'Shaughnessy, S. M., Deasy, M. J., Doyle, J. V., & Robinson, A. J. (2015). Performance analysis of a prototype small scale electricity-producing biomass cooking stove. *Applied energy*, 156, 566-576.
- [24] Toghyani, S., Ahmadi, M. H., Kasaeian, A., & Mohammadi, A. H. (2016). Artificial neural network, ANN-PSO and ANN-ICA for modelling the Stirling engine. *International Journal of Ambient Energy*, 37(5), 456-468.
- [25] Pourkiaei, S. M., Ahmadi, M. H., & Hasheminejad, S. M. (2016). Modeling and experimental verification of a 25W fabricated PEM fuel cell by parametric and GMDH-type neural network. *Mechanics & Industry*, 17(1), 105.
- [26] Ahmadi, M. H., Ahmadi, M. A., Mehrpooya, M., & Rosen, M. A. (2015). Using GMDH neural networks to model the power and torque of a stirling engine. *Sustainability*, 7(2), 2243-2255.
- [27] Ahmadi, M. H., Ahmadi, M. A., Sadatsakkak, S. A., & Feidt, M. (2015). Connectionist intelligent model estimates output power and torque of stirling engine. *Renewable and Sustainable Energy Reviews*, 50, 871-883.
- [28] Ahmadi, M. H., Aghaj, S. S. G., & Nazeri, A. (2013). Prediction of power in solar stirling heat engine by using neural network based on hybrid genetic algorithm and particle swarm optimization. *Neural Computing and Applications*, 22(6), 1141-1150.
- [29] Koten, H., Yilmaz, M., & Zafer Gul, M. (2014). Compressed biogas-diesel dual-fuel engine optimization study for ultralow emission. *Advances in Mechanical Engineering*, 6, 571063.
- [30] Yilmaz, M., Köten, H., & Gul, M. Z. (2012). Effects of the injection parameters and compression ratio on the emissions of a heavy-duty diesel engine. *International Journal of Vehicle Design*, 59(2/3), 147-163.
- [31] Anitha, A. A., Jayakumar, J., & Asirvatham, L. G. (2017). Performance analysis of (Bi₂Te₃-PbTe) hybrid thermoelectric generator. *International Journal of Power Electronics and Drive Systems*, 8(2), 917.
- [32] Khandelwal, S., & Chauhan, R. Y. (2013). Life cycle assessment of Neem and Karanja biodiesel: an overview. *International Journal of ChemTech Research*, 5(2), 659-665.
- [33] Chandra, R., Vijay, V. K., & Subbarao, P. M. V. (2009). Biogas production from de-oiled seed cakes of *Jatropha* and *Pongamia*. *Renewable Energy (Akshay Urja)*, 3(2), 17-22.

- [34] Radhakrishna, P. (2003). Tree borne oil seeds as a source of energy for decentralized planning. Government of India, Ministry of Non-Conventional Energy Sources, New Delhi, India.
- [35] "Clean Renewable Fuel from the Plasma Gasification of Waste", <http://www.waste-management-world.com>
- [36] Angeline, A. A., Jayakumar, J., Asirvatham, L. G., Marshal, J. J., & Wongwises, S. (2017). Power generation enhancement with hybrid thermoelectric generator using biomass waste heat energy. *Experimental Thermal and Fluid Science*, 85, 1-12.
- [37] Zhang, H. Y., Mui, Y. C., & Tarin, M. (2010). Analysis of thermoelectric cooler performance for high power electronic packages. *Applied thermal engineering*, 30(6-7), 561-568.
- [38] Chen, W. H., Liao, C. Y., Hung, C. I., & Huang, W. L. (2012). Experimental study on thermoelectric modules for power generation at various operating conditions. *Energy*, 45(1), 874-881.
- [39] <https://www.ashden.org/biomass-gasification>
- [40] Purohit, I., Purohit, P., & Shekhar, S. (2013). Evaluating the potential of concentrating solar power generation in Northwestern India. *Energy policy*, 62, 157-175.
- [41] "Renewable Energy Technologies: Cost Analysis series", <http://www.irena.org>, Power Sector, Vol.1, Issue 1/5, June 2012.
- [42] Sano, S., Mizukami, H., & Kaibe, H. (2003). Development of high-efficiency thermoelectric power generation system. Komatsu Technical Report, Report No.
- [43] Decker, B. Y., Calderon, S., & Gan, Y. (2015). Thermoelectric Properties of Bismuth Telluride Filled Silicone. *Journal of Thermal Engineering*, 1(6), 402-407.